IEEE Access
Multidisciplinary | Rapid Review | Open Access Journal

Received September 26, 2019, accepted October 14, 2019, date of publication November 6, 2019,
date of current version November 18, 2019.

Digital Object Identifier 10.1109/ACCESS.2019.2951947

Estimation and Utilization of Ground Effects on Conformal Dielectric Resonator Antennas

MA BOYUAN, JIN PAN, ENHAO WANG, AND DEQIANG YANG
School of Electronic Science and Engineering, University of Electronic Science and Technology of China, Chengdu 611731, China

Corresponding author: Jin Pan (jpuestc@163.com)

This work was supported by the Foundation for Innovative Research Group of the National Natural Science Foundation of China under Grant 61721001.

ABSTRACT Ground effects on arc-shaped conformal dielectric resonator antennas (DRAs) working in the $TE^{z}_{11\delta}$ mode are investigated and utilized to attain various radiation performances. Manipulation of directivity patterns are achieved with the help of the three-dimensional curved metal ground. The backlobe, beamwidth, broadside gain, backscattering, and cross-polarization level of the antenna are all readily controllable. The geometric theory of diffraction is applied to provide an intuitional explanation for the radiation changes. Detailed analysis is then conducted from the perspective of ground current. It is found that the current distribution is affected by configurations of both the arc DRA and ground plane. Based on this, analytical methods are developed to calculate the ground effects exclusively for conformal arc-shaped DRAs. Next, the design theory of arc DRAs with curved ground is proposed. To demonstrate it, two conformal DRAs owning directional and wide beams, respectively, are designed as paradigms. At last, a prototype is fabricated and measured for validation.

INDEX TERMS Conformal antennas, dielectric resonator antennas (DRAs), ground effects, radiation patterns.

I. INTRODUCTION

Dielectric resonator antennas (DRAs) enjoy wide bandwidth, compact size, little surface-wave or ohmic loss, and high degree of design freedom [1], [2]. Abundant theoretical and numerical methods have been developed to analyze DRAs on planar ground plane (GP), such as rectangular, cylindrical, hemisphere, triangular, annular, and sector DRAs, which boosts their application [1]–[4]. However, research on conformal DRAs on curved surface is incomplete. Though DRAs on nonplanar ground were exhibited in [5]–[8], the antennas themselves are scarcely conformal. In [9], we proposed theoretical models for convex and concave conformal DRAs, yet ignored the ground effect from the conformal metal plane.

Conformal antennas are preferable in electronic devices for vehicles, aircrafts, missiles, and wearable or implantable systems [10], [11]. These antennas are applied directly on the nonplanar surface of devices. Therefore, they enjoy low profile, compact size, and deployment flexibility. In conformal devices, the GP of antennas can be finite as an arc [9], closed as a sphere [5], or hybrid as a cylinder [6]. Traditional DRAs on nonplanar and flexible GP were presented in several studies [5]–[8], [12]–[15]. However, research in this field mainly focuses on exhibiting and utilizing specific phenomena. Systematical analysis and design principles are still required. Besides, ground effects on arc-shaped conformal DRAs are not included.

For DRAs on planar GP, the finite ground mainly influences the radiation pattern because of its violation of the image theory, excitation of surface wave, and scattering or diffraction [1], [2], [16]–[23]. Numerical methods [21], [22] were used to compute the ground effect precisely. With the help of commercial software, ground effects on DRAs were presented in [16]–[20]. In [19], the author proposed that the radiation from small planar GP with quasi-uniformly distributed surface current was complementary to that of the DRA on it. DRAs with low back lobe and high foreside gain were then designed. Instead of computing precise numerical solutions, this method explains the ground effect in a more intuitional way. Nonetheless, it focuses mainly on the CoP pattern and symmetrical planar GP with compact size. In [20], effects from planar substrate on XP level were studied through experiment. The author in [23] applied the geometric theory of diffraction (GTD) to analyze the planar ground.

The associate editor coordinating the review of this manuscript and approving it for publication was Haiwen Liu.

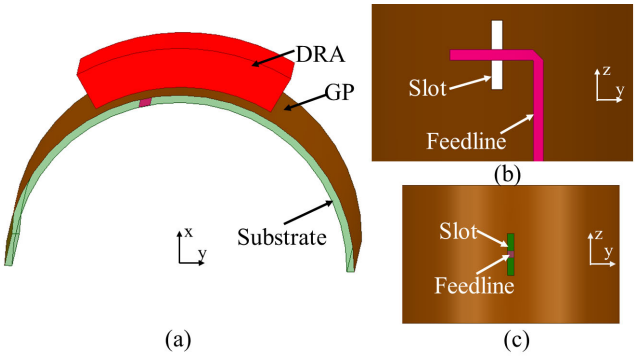

FIGURE 1. Slot-fed arc-shaped DRA. (a) DRA and substrate. (b) Feedline. (c) Feeding slot.

Although high-frequency asymptotic methods are more suitable for electrically large objects, they help to explain the radiation mechanism of the metal ground. However, this method is not sufficient when GP is conformal because it only considered the edge diffraction.

In this article, the effect of finite curved ground on an arc-shaped DRA operating in its $TE^z_{11\delta}$ mode is investigated and utilized. The ground effect on radiation patterns is presented, and then analyzed through the GTD and ground current. Both the co-polarization (CoP) and cross-polarization (XP) radiation are under consideration. Next, analytical methods are developed exclusively for convex DRAs with curved ground to estimate the radiation variation. Therefore, the pattern distortion for conformal DRAs placed on actual platforms is predictable. Moreover, explicit design steps are proposed to utilize the ground effect in achieving required radiation patterns. As paradigms, a directional and a wide-beam arc DRA are designed. Finally, a prototype is fabricated and measured for validation.

II. GROUND EFFECT ANALYSIS

In this section, ground effects on the radiation performance of an arc DRA is investigated both qualitatively and quantitatively. The conformal metal ground is assumed to have an arc shape. The two basic modes of arc DRAs [9] are of interest because of their popularity. The influence from z-directional dimensional change is found analogous to that in conventional planar DRAs [20], [23], [24]. Thus, we focus on the effect introduced by the φ-directional curved structure for brevity However, because the bending structure only exists in φ-direction, effects from the conformal ground on the $TM^z_{11\delta}$ mode [9] is similar to that on conventional flat-bottomed DRAs [19]. Thus, only the $TE^z_{11\delta}$ mode is considered in this work.

A. ANTENNA CONFIGURATION

A prototypical arc-shaped DRA on a conformal substrate is presented in Fig. 1. It operates in $TE^z_{11\delta}$ mode [9], of which electrical field (E-Field) and magnetic field (H-Field) are illustrated in Fig.2. The initial resonant frequency is calculated by the analytical model of arc DRAs in [9]. The antenna

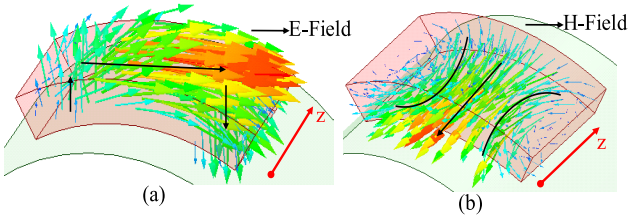

FIGURE 2. $TE^z_{11\delta}$ mode of arc-shaped DRA. (a) E-Field. (b) H-Field.

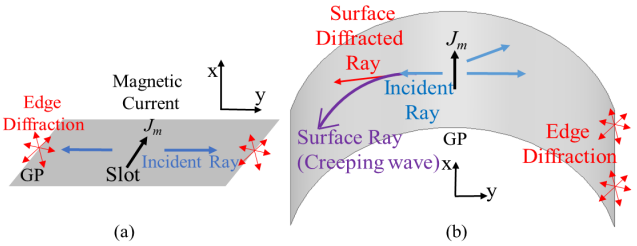

FIGURE 3. Radiation mechanism of DRAs on finite ground. (a) With planar ground. (b) With arc ground.

is excited through a slot under it, which is coupled through a Γ-shaped microstrip line below. The feeding port is at the edge of the substrate with an offset angle. The DRA is made of ceramic material ($\varepsilon_r = 12.3$, $tan\delta = 0.00014$).

B. CURVED GROUND

Given that a DRA working in its basic modes radiates like a magnetic dipole [1], the radiation mechanisms of planar and convex arc DRA are illustrated by the GTD, as seen in Fig. 3. From the perspective of electromagnetic rays, this theory provides a clear view of the ground effect on the radiation performance. For planar ground, diffraction effect is mainly ascribed to edges [23]. However, on arc-shaped ground, besides edge diffraction, surface diffraction appears because of the smooth convexity. When the ground is annular, φ-directional edge diffraction disappears. As for concave ground [9], reflection occurs because of the concavity.

As shown in Fig. 3 (b), the creeping wave [25] propagates along curved paths as surface rays, meanwhile, emits outgoing surface diffracted rays towards the tangential direction. According to the superposition principle and GTD, the total radiated field can be expressed as [26]

$$\begin{aligned} E_{light}(\mathbf{r}_l) + E_{shadow}(\mathbf{r}_s) &= E_{total}(\mathbf{r}) = E_i(\mathbf{r}) + E_r(\mathbf{r}) + E_d(\mathbf{r}) \\ &= E_i(\mathbf{r}_l) + 0 + E_{Ed}(\mathbf{r}) + E_{Sd}(\mathbf{r}) \end{aligned} \quad (1)$$

where E_{light} and E_{shadow} represent field in the light and shadow region. E_i, E_r, and E_d denote the incident, reflected, and diffracted field, respectively. Because the incident source is on the surface, the reflected field is null [25], and the incident field needs recalculating according to the surface dimension [26]. The diffracted field is attributed to the edges (E_{Ed}) and curved surface (E_{Sd}). The existence of diffracted rays may guide the radiated power to the squint side, resulting in wider, tilted, or even split beams.

Typical radiation variation due to changes in ground radian is shown in Fig. 4 and Table 1. When the GP is sym-

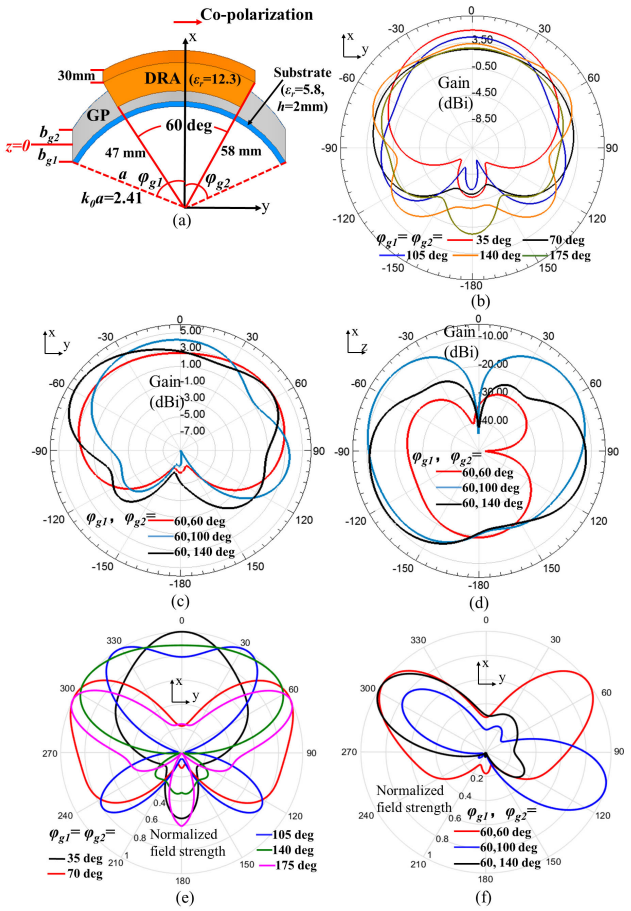

FIGURE 4. Radiation pattern with varying ground radian. (a) Ground configuration. (b)(c) Co-polarization in E-plane. (d) Cross-polarization in xoz plane. (e)(f) Calculated ground effects by (2).

TABLE 1. Typical radiation characteristics.

Ground radian		Radiation characteristics in ***xoy* plane**	
φ_{g1} (deg)	φ_{g2} (deg)	Co-polarization	Cross-polarization
35	35	High foreside gain	Below -18 dB
70	70	Wide beam	Below -18 dB
105	105	High backscattering	Below -18 dB
140	140	Wide beam, high backscattering	Below -18 dB
175	175	Wide beam, high backlobe	Below -18 dB
Asymmetrical ground			
φ_{g1} (deg)	φ_{g2} (deg)	CoP in ***xoy* plane**	XP in ***xoz* plane**
60	60	Wide symmetrical beam	Below -18 dB
60	100	Squint beam	8-dB degradation
60	140	Squint beam	8-dB degradation

metrical in φ-direction, its size affects the radiation pattern of co-polarization (CoP) drastically, in terms of broadside gain, back lobe, backscatter, and beamwidth, while cross-polarization (XP) level stays below -18 dB. According to Fig. 5 (a), small GP radiates like a y-directional electrical

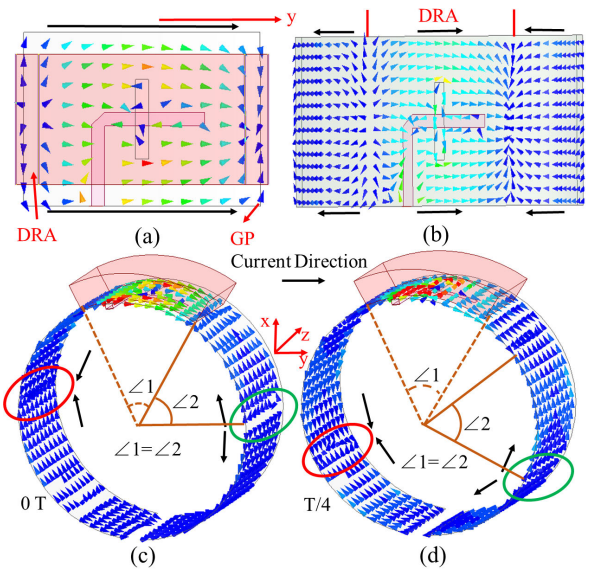

FIGURE 5. Ground current. (a) Current distribution on small and (b) large ground. (c) Current distribution at 0·T. (d) Current distribution at T/4.

dipole, which is complementary to the DRA [19]. Therefore, high foreside ($+x$) gain and a low back lobe ($-x$) are obtained [16]–[19]. As ground radian becomes larger, the surface current shows periodical variation, as illustrated in Fig. 5 (b)-(d). The current distribution resembles a long arc-shaped current sheet, of which periodicity complies with the DRA size. According to [24], the center-excited long arc-shaped ground current may have a radiation pattern with two symmetrical (to x-axis) squint beams in xoy plane, which explains the beam widening in Fig. 4 (b).

Asymmetrical GP deviates the CoP beam and causes extreme XP degradation, as presented in Fig. 4 (c) and (d). For symmetrical GP, the XP level is below -20 dB. The asymmetry may lead to an increase in XP level of more than 10 dB. The XP radiation pattern is distorted as well. This indicates that in certain direction, a XP degradation of dozens of dB could appear, which is catastrophic for applications under specific standard or interference restriction. Similar phenomena are rarely observed in conventional planar DRAs, because vertical ground current hardly exists in two-dimensional structures. The x-directional component of the ground current, seen in Fig 5. (b)-(d), generates vertically polarized electromagnetic wave at z-direction. When GP is symmetrical in φ-direction, the bilateral vertical currents have equal amplitude and opposite phase, and therefore, cancels each other. Nonetheless, with asymmetrical GP, the mutual cancellation disappears, resulting in the XP degradation in Fig. 5 (d).

C. GROUND EFFECT ESTIMATION

Two simple methods are presented to conduct a fast estimation of the ground effect on radiation performance. They are established for convex arc-shaped metal ground for its popularity, but also apply to annular and concave ones after

minor modification. The first method is purely experiment-based. Performance of arc DRAs with different ground plane is simulated by commercial software. Typical data are processed and exhibited in **Appendix**. The influence of curved GP is thus evaluable.

An analytical method for the estimation of the ground effect on radiation performance is developed based on the ground current distribution presented in Fig. 5. The ground is assumed in convex arc shape. For an enclosed annular or a concave one, the mechanism is different, yet analogous. Due to surface diffraction and edge reflection [25], the creeping current is of evanescent travelling-standing type. Driven by the arc DRA, the surface current exhibits periodicity which is dominated by the radian of the centered antenna, as illustrated in Fig. 5 (c) and (d). Similar characteristics are also observed in the prototypes in [9]. Therefore, the radiation in E-plane from the ground current is approximated by (2),

$$\begin{aligned} E_\varphi(\varphi) &= C(r)[E_{Surf}(\varphi) + E_{Edge}(\varphi)] \\ &= -j\omega\frac{\mu_0}{4\pi}\frac{e^{-jkr}}{r}\int_{-\varphi_{g1}}^{\varphi_{g2}} I_{total}(\varphi')F_{total}(\varphi-\varphi') \\ &\quad \times e^{jka\cos(\varphi-\varphi')}d\varphi' \\ &= \frac{-j\omega\mu_0 e^{-jkr}}{4\pi r}\int_{-\varphi_{g1}}^{\varphi_{g2}} e^{jka\cos(\varphi-\varphi')} \\ &\quad \times \{I_{surf}(\varphi')F_{surf}(\varphi-\varphi') + I_{edge}(\varphi')F_{edge}(\varphi-\varphi') \\ &\quad \times [\delta(\varphi'+\varphi_{g1}) + \delta(\varphi'-\varphi_{g2})]\}d\varphi' \end{aligned} \tag{2}$$

where

$$\begin{aligned} I_{surf}(\varphi) &= I^+ - R\cdot I^- = I_0[e^{-\alpha|\varphi|}e^{-j\beta|\varphi|} \\ &\quad - Re^{\alpha(|\varphi|-2\varphi_{g1,2})}e^{j\beta(|\varphi|-2\varphi_{g1,2})}]; \\ I_{edge}(\varphi) &= D\cdot I_0 e^{-(\alpha+j\beta)|\varphi|};\ \beta = \frac{\pi}{\varphi_{dr}};\quad D^2+R^2=1; \\ F_{surf}(\varphi) &= \cos\varphi\cdot u(|\varphi|-\frac{\pi}{2});\quad F_{edge}(\varphi) = \cos\varphi \end{aligned}$$

where $C(r)$ is the pattern factor independent of the ground dimension, k is the wavenumber in free space, a is the radius of the arc ground, φ_{g1} and φ_{g2} represent the radian of the arc while φ_{dr} is that of the DRA, α characterizes the surface diffraction, D and R describe the diffraction and reflection at the two edges, and $\delta(x)$ and $u(x)$ are the impulse and step functions, respectively. It should be noticed that the effective phase constant β is decided by the DRA radian. The surface and edge diffraction, and first-order reflection at the ground fringe are all under consideration. They can be obtained based on [25] and [26], or simple curve fitting.

Ground effects are calculated as seen in Fig. 4 (e) and (f). The results explain the beam characteristics and variation tendency in the simulated radiation patterns shown in Fig. 4(b), (c), and Appendix.

As to the ground effect on XP in Fig. 4 (c), an analytical estimating method associated with the ground width, b_{g1} and b_{g2} is obtained, as seen in (3).

$$\begin{aligned} &E_{\theta_x}(\theta_x) \\ &= C(r,\theta_x)[E_{EdgeZ} + E_{EdgeY}] \\ &= (e^{-jk_0 b_{g1}\sin\theta_x} + e^{jk_0 b_{g2}\sin\theta_x})j\omega\sin\theta_x\frac{\mu_0}{4\pi}\frac{e^{-jkr}}{r} \\ &\quad \times\int_{-\varphi_{g1}}^{\varphi_{g2}} I_{\varphi_{total}}(\varphi')\sin(|\varphi'|)F_{total}(\theta_x)e^{jka\cos\theta_x\cos\varphi'}d\varphi' \\ &= (e^{-jk_0 b_{g1}\sin\theta_x} + e^{jk_0 b_{g2}\sin\theta_x})j\omega\sin\theta_x\frac{\mu_0}{4\pi}\frac{e^{-jkr}}{r} \\ &\quad \times\int_{-\varphi_{g1}}^{\varphi_{g2}} \sin(|\varphi'|)e^{jka\cos\theta_x\cos\varphi'}\{I_{EdgeZ}(\varphi')F_{EdgeZ}(\theta_x) \\ &\quad + I_{EdgeY}(\varphi')F_{EdgeY}(\theta_x)[\delta(\varphi'+\varphi_{g1}) + \delta(\varphi'-\varphi_{g2})]\}d\varphi' \end{aligned} \tag{3}$$

where

$$\begin{aligned} I_{EdgeZ}(\varphi) &= I^+ - R\cdot I^- = I_0[e^{-\alpha|\varphi|}e^{-j\beta|\varphi|} \\ &\quad - Re^{\alpha(|\varphi|-2\varphi_{g1,2})}e^{j\beta(|\varphi|-2\varphi_{g1,2})}]; \\ I_{EdgeY}(\varphi) &= D\cdot I_0 e^{-(\alpha+j\beta)|\varphi|};\ \beta = \frac{\pi}{\varphi_{dr}};\ D^2+R^2=1; \\ F_{EdgeZ}(\theta_x) &= \sin\theta_x;\ F_{EdgeY}(\theta_x) = \sin\theta_x; \end{aligned}$$

Symbols in (3) have the same meaning as those in (2). The subscript of θ indicates that the equation is formulized based on x-axis.

III. DESIGN THEORY EMPLOYING GROUND EFFECTS

A. DESIGN GUIDE

Based on the above analysis, concise design steps are obtained for a slot-fed convex arc-shaped DRA on conformal GP. It can attain various radiation requirements.

The DRA works in its $TE^z_{11\delta}$ mode [9], and the GP is assumed symmetrical. If asymmetrical GP is preferred or inevitable, XP radiation pattern should be estimated through (3) in advance, and be checked repeatedly during simulation. The design procedure is shown below.

a) Compute the antenna size based on its operating frequency and available material by the equations in [9].
b) Verify and modify the theoretical design with the help of eigenmode or characteristic mode solvers.
c) Decide substrate thickness based on demand, cost, and availability, and then calculate the size of feeding structure based on [1] and [2].
d) Determine the initial radian of the GP through (2) according to the required radiation pattern in E-plane. The radiation from the GP is estimated by (2) or the data in Appendix. Small GP ($\varphi_{g1}+\varphi_{g2} = 1$ to $1.5\,\varphi_{dr}$) contributes to high broadside gain and low back lope, while large one ($\varphi_{g1}+\varphi_{g2} > 2\varphi_{dr}$) guides the beam to its extension direction.
e) Regard the two edges in z-direction and DRA with a leaky slot below as two three-element linear arrays [23]–[26] towards upper and lower sides, respectively. Then, determine the GP size depending on radiation requirements.

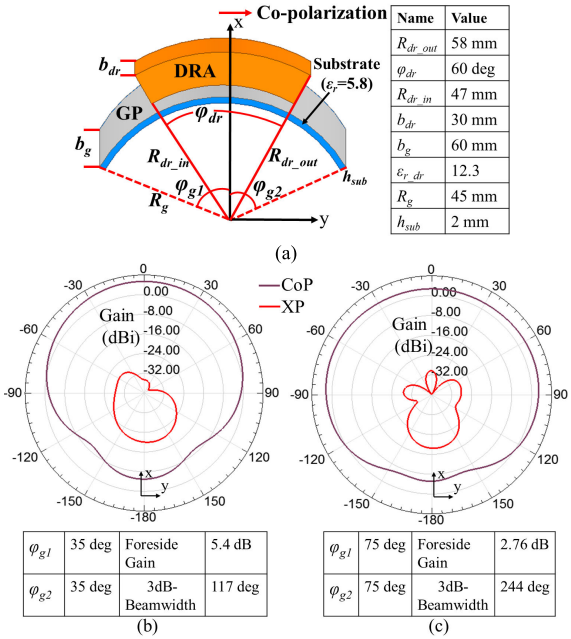

Name	Value
R_{dr_out}	58 mm
φ_{dr}	60 deg
R_{dr_in}	47 mm
b_{dr}	30 mm
b_g	60 mm
ε_{r_dr}	12.3
R_g	45 mm
h_{sub}	2 mm

φ_{g1}	35 deg	Foreside Gain	5.4 dB
φ_{g2}	35 deg	3dB-Beamwidth	117 deg

(b)

φ_{g1}	75 deg	Foreside Gain	2.76 dB
φ_{g2}	75 deg	3dB-Beamwidth	244 deg

(c)

FIGURE 6. Design examples. (a) Antenna Configuration. (b) Directional antenna. (c) Wide-beam antenna.

Small GP ($b_{g1} + b_{g2} = 1$ to $1.5\ b_{dr}$) helps in backlobe reduction, whereas larger one ($b_{g1} + b_{g2} > 2b_{dr}$) may bring higher gain at both foreside and backside.

f) Simulation and optimization.

B. DESIGN EXAMPLES

To demonstrate the design strategy, two conformal DRAs with different radiation patterns are proposed, as seen in Fig. 6. The two DRAs are supposed to operate in the $TE^z_{11\delta}$ mode shown in Fig. 2 around 2.45 GHz. As seen in Fig. 6(a), their size is calculated by the method in [9]. Then, a commercial eigenmode solver is used to check their internal field. According to the field distribution in Fig. 2, the feeding structure shown in Fig. 1 (b) is applied so that strong coupling exists between the slot and DRA [2]. We assumed that the first arc DRA needed a directional radiation pattern for communication devices, whereas the other one requires an extremely wide beam for applications like navigational systems. Therefore, the ground radian is determined by (2), and then optimized through simulation. As seen in Fig. 6(b) and (c), two distinct patterns are obtained with exactly the same DRA size. The directional antenna has a gain of 2.7 dB higher than that of the other one. Whereas the wide-beam DRA has a 3dB-beamwidth of 244 degree, which is more than two times larger than that of the directional antenna.

IV. FABRICATION AND MEASUREMENT

A slot-fed arc-shaped DRA on conformal ground is fabricated and measured for validation, as presented in Fig. 7. The DRA and substrate were truncated from annular ceramic blocks. The feedline, GP, and slot were printed onto the substrate by silk-screen printing with molecular silver paste. Copper wings at the margins of GP were added to adjust its

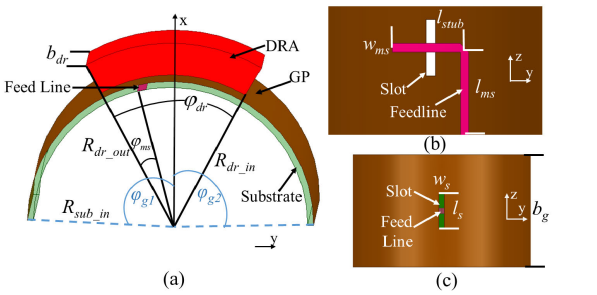

R_{dr_out}	58 mm	ls	18.73 mm	l_{ms}	52.88 mm	φ_{g1}	35 deg
R_{dr_in}	47 mm	w_s	3.08 mm	w_{ms}	2.83 mm	φ_{g2}	35 deg
b_{dr}	30 mm	R_{sub_in}	45 mm	l_{stub}	12.88 mm	ε_{r_dr}	12.3
φ_{dr}	60 deg	b_g	80 mm	φ_{ms}	16.1 deg	ε_{r_sub}	5.8

FIGURE 7. Antenna prototype. (a) Designed DRA. (b) Feedline. (c) Feeding slot.

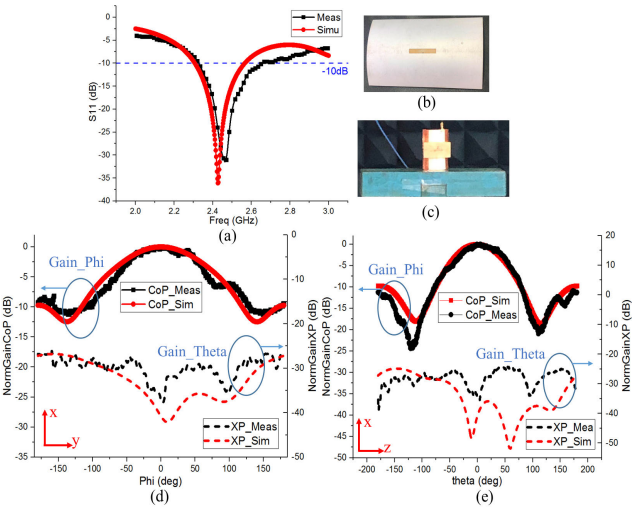

FIGURE 8. Measurement and results. (a) S parameter. (b) Feeding structure. (c) Antenna under test. (d) E-plane and (e) H-plane pattern of co- and cross-polarization.

dimension. The DRA and substrate were bonded together by epoxy glue ($\varepsilon_r \sim 3.6$). A SMA connector was welded at the edge for measurement. The antenna was then measured with a vector network analyzer and a far-field microwave anechoic chamber. The results are presented in Fig. 8. The DRA resonates around 2.45 GHz, with a simulated and measured bandwidth of 11.11% and 14.2%, respectively. Its simulated and measured gain is 5.6 dB and 5 dB. The XP level is below -25 dB in E-plane and -28 dB in H-plane.

V. CONCLUSION

Ground effects on arc-shaped conformal DRAs have been investigated and utilized to manipulate radiation patterns. The curved GP has been proved to have significant influence on the broadside gain, backscatter, beamwidth, backlobe, and XP level of an arc DRA. Symmetrical GP mainly affects the radiation pattern of CoP, while asymmetrical one can cause beam deviation and severe XP-level degradation. These phenomena have been explained theoretically based on the

TABLE 2. Typical Ground Effects on Radiation Performance I (corresponding to Fig. 4 (a)).

	k_0a	$\varphi_{g1}/\varphi_{dr}$	$\varphi_{g2}/\varphi_{dr}$	k_0b_{g1}	k_0b_{g2}	Radiation pattern
A1	2.43	0.5	0.5	1.54	1.54	
A2	2.43	0.75	0.75	1.54	1.54	
A3	2.43	1	1	1.54	1.54	
A4	2.43	1.25	1.25	1.54	1.54	
A5	2.43	1.5	1.5	1.54	1.54	
A6	2.43	1.75	1.75	1.54	1.54	
A7	2.43	2	2	1.54	1.54	
A8	2.43	2.25	2.25	1.54	1.54	
A9	2.43	2.5	2.5	1.54	1.54	
A10	2.43	2.75	2.75	1.54	1.54	
B1	2.43	0.58	0.58	1.03	1.03	
B2	2.43	0.58	0.58	1.28	1.28	
B3	2.43	0.58	0.58	1.54	1.54	
B4	2.43	0.58	0.58	1.80	1.80	
B5	2.43	0.58	0.58	2.05	2.05	
B6	2.43	0.58	0.58	2.31	2.31	
B7	2.43	0.58	0.58	2.57	2.57	
B8	2.43	0.58	0.58	2.82	2.82	
B9	2.43	0.58	0.58	3.08	3.08	
B10	2.43	0.58	0.58	3.34	3.34	
C1	2.43	0.67	1.33	1.54	1.54	
C2	2.43	0.67	2	1.54	1.54	
C3	2.43	0.67	2.67	1.54	1.54	
C4	2.43	1.5	0.83	1.54	1.54	
C5	2.43	1.5	2	1.54	1.54	
C6	2.43	1.5	2.67	1.54	1.54	
D1	2.43	0.5	0.5	1.03	2.05	
D2	2.43	0.75	0.75	1.03	3.59	
D3	2.43	1	1	1.03	4.10	
D4	2.43	1.25	1.25	1.54	2.57	
D5	2.43	1.5	1.5	2.57	3.59	
D6	2.43	1.75	1.75	2.57	4.10	

TABLE 3. Typical Ground Effects on Radiation Performance II (corresponding to Fig. 4 (a)).

k_0a=2.43		$\varphi_{g1}/\varphi_{dr}$	$\varphi_{g2}/\varphi_{dr}$	k_0b_{g1}	k_0b_{g2}	Maximum gain (dB)	Beam type	3-dB Beam-width (deg)	Backward gain (dB)	Maximum backscatter (dB)	Maximum XP gain (dB)
A1	2.43	0.5	0.5	1.54	1.54	5.4	Broadside	108.96	-3.6	-1.8	<-18
A2	2.43	0.75	0.75	1.54	1.54	4.2	Broadside	177.37	-7.7	1.3	<-18
A3	2.43	1	1	1.54	1.54	3.4	Broadside	230.09	-5.9	2.6	<-18
A4	2.43	1.25	1.25	1.54	1.54	3.1	Broadside	243.81	-5.2	2.7	<-18
A5	2.43	1.5	1.5	1.54	1.54	3.9	Broadside	229.78	-5.2	2.1	<-18
A6	2.43	1.75	1.75	1.54	1.54	4.3	Broadside	106.16	-6.2	2.0	<-18
A7	2.43	2	2	1.54	1.54	3.9	Broadside	147.57	-8.6	2.5	<-18
A8	2.43	2.25	2.25	1.54	1.54	4.4	Split	162.35	-4.6	2.3	<-18
A9	2.43	2.5	2.5	1.54	1.54	4.0	Split	174.47	-1.6	1.2	<-18
A10	2.43	2.75	2.75	1.54	1.54	3.6	Broadside	181.67	0.16	0.9	<-18
B1	2.43	0.58	0.58	1.03	1.03	4.9	Broadside	127.48	-6.8	-0.7	<-18
B2	2.43	0.58	0.58	1.28	1.28	5.1	Broadside	111.02	-6.1	-2.1	<-18
B3	2.43	0.58	0.58	1.54	1.54	5.3	Broadside	97.62	-5.0	-3.8	<-18
B4	2.43	0.58	0.58	1.80	1.80	5.5	Broadside	89.43	-4.0	-4.0	<-18
B5	2.43	0.58	0.58	2.05	2.05	5.7	Broadside	81.52	-3.3	-3.3	<-18
B6	2.43	0.58	0.58	2.31	2.31	5.7	Broadside	78.32	-3.2	-3.2	<-18
B7	2.43	0.58	0.58	2.57	2.57	5.7	Broadside	74.38	-3.2	-3.2	<-18
B8	2.43	0.58	0.58	2.82	2.82	5.6	Broadside	75.52	-3.3	-3.3	<-18
B9	2.43	0.58	0.58	3.08	3.08	5.2	Broadside	87.5	-2.4	-2.1	<-18
B10	2.43	0.58	0.58	3.34	3.34	4.8	Broadside	110.76	-1.7	-1.3	<-18
C1	2.43	0.67	1.33	1.54	1.54	4.8	Squint	124.34	-7.1	0.4	-8.9
C2	2.43	0.67	2	1.54	1.54	3.6	Squint	190.59	-6.3	2.5	-10.1
C3	2.43	0.67	2.67	1.54	1.54	4.7	Squint	120.13	-3.4	0.4	-9.2
C4	2.43	1.5	0.83	1.54	1.54	4.0	Squint	190.40	-2.2	1.0	-14.2
C5	2.43	1.5	2	1.54	1.54	4.4	Squint	161.76	-5.2	1.4	-13.0
C6	2.43	1.5	2.67	1.54	1.54	4.7	Squint	99.24	-6.3	0.6	-11.6
D1	2.43	0.5	0.5	1.03	2.05	5.3	Squint	113.46	-4.1	0.0	-6.5
D2	2.43	0.75	0.75	1.03	3.59	5.3	Squint	89.44	-3.7	-1.6	-16.7
D3	2.43	1	1	1.03	4.10	5.5	Squint	100.30	-3.4	-1.4	-7.6
D4	2.43	1.25	1.25	1.54	2.57	5.0	Squint	102.08	-3.5	-1.0	-15
D5	2.43	1.5	1.5	2.57	3.59	5.3	Squint	95.02	-3.8	-2.4	-9.5
D6	2.43	1.75	1.75	2.57	4.10	4.5	Squint	124.57	-6.0	-2.9	-5.4

GTD and ground current. Analytical equations have also been derived to estimate the ground effect based on both the DRA and ground configurations. Radiation variation of conformal DRAs applied on practical platforms is thus predictable. Furthermore, an explicit design method for conformal DRAs with arc ground has been proposed. Through this method, diverse radiation characteristics are attainable, such as a beamwidth varying from 117 to 244 degree. Further research may include ground effects on concave DRAs, or convex ones working in other modes.

APPENDIX

See Table 2 and Table 3.

REFERENCES

[1] K. M. Luk and K.W. Leung, Eds., *Dielectric Resonator Antennas*. Baldock, U.K.: Research Studies Press, 2003.
[2] A. Petosa, *Dielectric Resonator Antenna Handbook*. Norwood, MA, USA: Artech House, 2007.
[3] S. K. K. Dash, T. Khan, and A. De, "Dielectric resonator antennas: An application oriented survey," *Int. J. RF Microw. Comput.-Aided Eng.*, vol. 27, no. 3, Mar. 2017, Art. no. e21069, doi: 10.1002/mmce.21069.
[4] S. K. K. Dash, T. Khan, and Y. M. M. Antar, "A state-of-art review on performance improvement of dielectric resonator antennas," *Int. J. RF Microw. Comput.-Aided Eng.*, vol. 28, Aug. 2018, Art. no. e21270, doi: 10.1002/mmce.21270.
[5] S. H. Zainud-Deen, N. A. El-Shalaby, and K. H. Awadalla, "Hemispherical dielectric resonator antenna mounted on or embedded in spherical ground plane with a superstrate," in *Proc. NRSC*, Cairo, Egypt, Apr. 2011, pp. 1–9.
[6] H. Chorfi, M. Nedil, I. B. Mabrouk, T. A. Denidni, and L. Talbi, "Design of a 60 GHz dielectric resonator antenna array mounted on a conformal structure," in *Proc. IEEE Int. Symp. Antennas Propag. (APSURSI)*, Chicago, IL, USA, Jul. 2012, pp. 1–2.
[7] S. H. Zainud-Deen, M. S. Ibrahim, and A. Z. Botros, "High-directive dielectric resonator antenna over curved ground plane using metamaterials," in *Proc. NRSC*, Cairo, Egypt, Apr. 2011, pp. 1–9.
[8] H. Chorfi, M. Nedil, Y. Coulibaly, T. A. Denidni, I. B. Mabrouk, and L. Talbi, "A dielectric resonator antenna mounted on a conformal structure at 60 GHz," in *Proc. APSURSI*, Spokane, WA, USA, Jul. 2011, pp. 2577–2580.
[9] M. Boyuan, J. Pan, E. Wang, and Y. Luo, "Conformal bent dielectric resonator antennas with curving ground plane," *IEEE Trans. Antennas Propag.*, vol. 67, no. 3, pp. 1931–1936, Mar. 2019.
[10] E. Rodriguez-Villegas, S. Iranmanesh, and S. A. Imtiaz, "Wearable medical devices: High-level system design considerations and tradeoffs," *IEEE Solid State Circuits Mag.*, vol. 10, no. 4, pp. 43–52, Nov. 2018.
[11] Y. Liu, H. Yang, Z. Jin, and J. Zhu, "Circumferentially conformal slot array antenna and its Ka-band multibeam applications," *IET Microw., Antennas Propag.*, vol. 12, no. 15, pp. 2307–2312, Dec. 2018.
[12] M. M. Tahseen and A. A. Kishk, "Textile-based wideband flexible wearable dielectric resonator antennas for WLAN-band," in *Proc. 17th ANTEM*, Montreal, QC, Canada, Jul. 2016, pp. 1–3.
[13] A. Iqbal and O. A. Saraereh, "Design and analysis of flexible cylindrical dielectric resonator antenna for body centric WiMAX and WLAN applications," in *Proc. Loughborough Antennas Propag. Conf. (LAPC)*, Loughborough, U.K., Nov. 2016, pp. 1–4.
[14] S. H. H. Mashhadi, Z. Wu, and L. Z. Thamae, "Investigation of a wearable broadband textile dielectric resonator antenna," in *Proc. Loughborough Antennas Propag. Conf.*, Loughborough, U.K., Nov. 2010, pp. 349–352.
[15] S. H. H. Mashhadi, S. M. Y. Abbas, Z. Wu, and L. Z. Thamae, "Transmission characteristics of wearable broadband textile dielectric resonator antennas in body area network," in *Proc. 9th Int. Bhurban Conf. Appl. Sci. Technol. (IBCAST)*, Islamabad, Pakistan, Jan. 2012, pp. 336–339.
[16] L. Guo and K. W. Leung, "Compact linearly and circularly polarized unidirectional dielectric resonator antennas," *IEEE Trans. Antennas Propag.*, vol. 64, no. 6, pp. 2067–2074, Jun. 2016.
[17] L. Guo, K. W. Leung, and N. Yang, "Wide-beamwidth unilateral dielectric resonator antenna using higher-order mode," *IEEE Trans. Antennas Propag.*, vol. 18, no. 1, pp. 93–97, Jan. 2019.
[18] P. F. Hu, Y. M. Pan, X. Y. Zhang, and B. J. Hu, "A compact quasi-isotropic dielectric resonator antenna with filtering response," *IEEE Trans. Antennas Propag.*, vol. 67, no. 2, pp. 1294–1299, Feb. 2019.
[19] Y. M. Pan, K. W. Leung, and K. Lu, "Compact quasi-isotropic dielectric resonator antenna with small ground plane," *IEEE Trans. Antennas Propag.*, vol. 62, no. 2, pp. 577–585, Feb. 2014.
[20] A. K. Ojha and P. K. A. Vijayaraghavan, "Substrate size selection of microstrip-fed cylindrical dielectric resonator antennas for lowering the cross-polarisation," *IET Microw., Antennas Propag.*, vol. 13, no. 2, pp. 246–251, Feb. 2019.
[21] R. M. Baghaee, H. M. Neshati, and J. R. Mohassel, "Rigorous analysis of rectangular dielectric resonator antenna with a finite ground plane," *IEEE Trans. Antennas Propag.*, vol. 56, no. 9, pp. 2801–2809, Sep. 2008.
[22] N. V. Larsen and O. Breinbjerg, "Two-stage MAS technique for analysis of DRA elements and arrays on finite ground planes," *Electron. Lett.*, vol. 43, no. 12, pp. 657–659, Jun. 2007.
[23] A. Petosa, "Ferrite and dielectric antennas for personal communications," Ph.D. dissertation, Dept. Electron., Carleton Univ., Ottawa, ON, Canada, 1995.
[24] J. D. Kraus and R. J. Marhefka, *Antennas for All Applications*, 3rd ed. New York, NY, USA: McGraw-Hill, 2002.
[25] M. Wang, *Geometric Theory of Diffraction*, 2nd ed. Xi'an, China: Xidian Univ. Press, 1994.
[26] N. Wang, *Modern Uniform Geometrical Theory of Diffraction*. Xi'an, China: Xidian Univ. Press, 2010.
[27] A. Y. Svezhentsev and G. A. E. Vandenbosch, "Spatial Green's function singularity for sheet electric current over dielectric coated cylinder," *IEEE Trans. Antennas Propag.*, vol. 52, no. 2, pp. 608–610, Feb. 2004.

MA BOYUAN was born in Changchun, Jilin, China, in 1993. He received the B.S. degree in electromagnetic field and wireless technology from Yingcai Honor College, University of Electronic Science and Technology of China, Chengdu, China, in 2016, where he is currently pursuing the Ph.D. degree with the School of Electronic Science and Engineering. His current research interest includes theory and design of dielectric resonator antennas.

JIN PAN received the B.S. degree in electronics and communication engineering from the Radio Engineering Department, Sichuan University, Chengdu, China, in 1983, and the M.S. and Ph.D. degrees in electromagnetic field and microwave technique from UESTC, in 1983 and 1986, respectively. From 2000 to 2001, he was a Visiting Scholar in electronics and communication engineering from the Radio Engineering Department, City University of Hong Kong. He is currently a Full Professor with the the School of Electronic Engineering, UESTC. His current research interests include electromagnetic theory and computation, antenna theory and technique, field and wave in inhomogeneous media, and microwave remote sensing theory and its applications.

ENHAO WANG received the B.S. degree in electromagnetic field and wireless technology from the Electronic Information Engineering Department, University of Electronic Science and Technology of China, Chengdu, China, in 2017, where he is currently pursuing the degree majoring in electronic and communication engineering. His current research interests include antenna theory and technique, and remote sensing theory and its applications.

DEQIANG YANG received the B.E., M.E., and D.E. degrees from the School of Electronic Science and Engineering, University of Electronic Science and Technology of China (UESTC), in 1992, 2006, and 2012, respectively. From 2012 to 2016, he was a Senior Engineer with UESTC. His research interests include UWB indoor localization technology, antenna measurement, and antenna theory.